

Special
Collection

Mechanistic Study of the Activation and the Electrocatalytic Reduction of Hydrogen Peroxide by Cu-tmpa in Neutral Aqueous Solution

Michiel Langerman and Dennis G. H. Hetterscheid*^[a]

This article is dedicated to the memory of Prof. Jean-Michel Savéant and his enormous contributions to molecular electrochemistry

Hydrogen peroxide plays an important role as an intermediate and product in the reduction of dioxygen by copper enzymes and mononuclear copper complexes. The copper(II) tris(2-pyridylmethyl)amine complex (Cu-tmpa) has been shown to produce H₂O₂ as an intermediate during the electrochemical 4-electron reduction of O₂. We investigated the electrochemical hydrogen peroxide reduction reaction (HPRR) by Cu-tmpa in a neutral aqueous solution. The catalytic rate constant of the

reaction was shown to be one order of magnitude lower than the reduction of dioxygen. A significant solvent kinetic isotope effect (KIE) of 1.4 to 1.7 was determined for the reduction of H₂O₂, pointing to a Fenton-like reaction pathway as the likely catalytic mechanism, involving a single copper site that produces an intermediate copper(II) hydroxo species and a free hydroxyl radical anion in the process.

1. Introduction


The formation, decomposition, and reduction of H₂O₂ plays an important role in many (bio)chemical processes, such as oxidation reactions,^[1] fuel cells chemistry,^[2] and enzymatic reactions. Many peroxidases and catalases scavenge and disproportionate H₂O₂ into O₂ and H₂O to prevent formation of reactive oxygen species (ROS) that induce damage to their hosts.^[3] In the context of elucidating the oxidative catalytic reactions taking place at the active sites of these enzymes, often containing copper, iron, or manganese ions, many synthetic mimic catalysts have been synthesized and studied intensively.^[4]


Of particular interest are lytic polysaccharide monoxygenases (LPMOs), a family of copper-containing enzymes that are able to degrade lignocellulosic biomass.^[5] Over the last decade, since the discovery of the LPMO family of enzymes, significant scientific effort has been put into the determination of the structure and active site of LPMOs. It was revealed that all LPMOs contain a type II copper centre as their active site in a Cu^{II} resting state, with little variation in the primary coordination sphere for the different LPMOs.^[5c,6] The primary coordina-


tion sphere is formed by the coordination of three N ligands in a T-shaped geometry around the copper centre, with the primary coordination sphere conforming to a trigonal-bipyramidal geometry. The N ligands comprise a monodentate histidine and a bidentate histidine, coordinating with both the imidazole and backbone nitrogen coordinating to the copper centre, the so-called histidine brace. Polysaccharides are cleaved by LPMOs through an oxidative mechanism, and it was shown that both O₂ and H₂O₂ can act as the oxidant. Additionally, in the absence of polysaccharide substrate, H₂O₂ is produced by the enzyme in the presence of O₂. This behaviour shows similarities to that of single site copper complexes, which can both reduce O₂ and H₂O₂, while also producing H₂O₂ as a detectable intermediate during catalysis.^[7] In this light, we have recently reported, the oxygen reduction reaction mediated by Cu-tmpa (tmpa = tris(2-pyridylmethyl)amine), which has a maximum turnover frequency $1.8 \times 10^6 \text{ s}^{-1}$ for the reduction of dioxygen and involved the formation of H₂O₂ during the catalytic cycle.^[7a] Density functional theory (DFT) calculations of LPMO systems have shown that the most likely catalytic species responsible for the cleavage of polysaccharides is a copper oxyl radical (Cu^{II}-O^{•-}) species. Several different routes have been suggested for the catalytic pathway.^[8] Fenton chemistry plays an important role in many of these processes, and it has been shown that Fenton-like reactions can take place between Cu^I complexes and H₂O₂, resulting in the homolytic cleavage of the O-O bond.^[9]

Another enzyme that shows similarities to both the LPMOs and single site copper complexes, is the particulate methane monoxygenase (pMMO), which activates and reduces dioxygen in order to oxidize methane to methanol. Many conflicting suggestions on the nature of the Cu₂ active site in pMMO have been proposed, which was either considered a mononuclear or dinuclear copper centre,^[6,10] but recent experimental work points towards a catalytic centre containing a mononuclear

[a] M. Langerman, Dr. D. G. H. Hetterscheid
Leiden Institute of Chemistry
Leiden University
P.O. Box 9502, 2300 RA Leiden, The Netherlands
E-mail: d.g.h.hetterscheid@chem.leidenuniv.nl

 Supporting information for this article is available on the WWW under <https://doi.org/10.1002/celec.202100436>

 An invited contribution to a joint Special Collection in memory of Prof. Jean-Michel Savéant

 © 2021 The Authors. ChemElectroChem published by Wiley-VCH GmbH. This is an open access article under the terms of the Creative Commons Attribution Non-Commercial NoDerivs License, which permits use and distribution in any medium, provided the original work is properly cited, the use is non-commercial and no modifications or adaptations are made.

copper ion in a square-pyramidal geometry and includes a histidine brace similar to the LPMOs.^[11]

How hydrogen peroxide is formed and activated are very important research questions, taking into account potential applications of this chemistry. In traditional polymer electrolyte membrane (PEM) fuel cells, formation of H₂O₂ is considered undesirable as it leads to both catalyst poisoning and damaging of the proton exchange membrane.^[2a,12] However, more recently hydrogen peroxide has also been suggested as an alternative sustainable fuel or oxidant in fuel cells, owing to the broad range of standard equilibrium potentials associated with H₂O₂.^[2d,13] Currently, the bulk of H₂O₂ is synthesized through the anthraquinone process, which uses several different catalysts (Pd or Ni), creates a significant amount of waste products, and requires expensive separation steps in order to obtain concentrated H₂O₂.^[14] As such, despite the use of H₂O₂ as a sustainable oxidant in many chemical reactions, its production is not sustainable.^[1c,15] An electrochemical synthesis by selective 2-electron reduction of O₂ at low overpotentials would be a more desirable approach to obtain H₂O₂.

Understanding how hydrogen peroxide is activated and reduced at copper sites is essential for our understanding of single site copper monooxygenases, and in potential the design of new catalysts for the oxygen reduction reaction and the electrochemical production of H₂O₂. In this study, we report our findings on the electrocatalytic behaviour of Cu-tmpa towards the hydrogen peroxide reduction reaction (HPRR) under neutral aqueous conditions, showing solvent kinetic isotope effects (KIE), rate orders, and catalytic rate constants. Based on this, we propose a catalytic mechanism for the Cu-tmpa catalysed HPRR.

2. Results and Discussion

2.1. Electrocatalytic Reduction of Hydrogen Peroxide by Cu-tmpa

The electrocatalytic reduction of H₂O₂ by Cu-tmpa in a phosphate buffer (PB) solution of pH 7, containing 100 mM phosphate salts (NaH₂PO₄ and Na₂HPO₄), was investigated in detail and the results are discussed here. In Figure 1a, a CV measured in the aforementioned solution in the presence of 1.1 mM H₂O₂ shows a peak-shaped catalytic wave. The catalytic half-wave potential ($E_{\text{cat}/2}$) of this catalytic wave is situated at 0.34 V vs. RHE, which is close to the $E_{\text{cat}/2}$ of the ORR at 0.33 V vs. RHE observed under stationary conditions. For both the HPRR and the ORR a catalytic peak potential of 0.26 V was found, which suggests that both ORR and HPRR may be limited by side phenomena such as mass transport limitations. Additionally, a comparison of the CVs of the electrochemical reduction of H₂O₂ and O₂ reveals that the peak catalytic current (i_{cat}) for the HPRR (30 μA) is less than a third of that of ORR (100 μA), as shown in Figure 1b. While a lower i_{cat} can be an indication of a slower catalytic reaction, this only holds true if the substrate and the catalytic mechanism are the same when comparing CV measurements. This is clearly not the case for the ORR and HPRR, and the large difference in peak catalytic current can be

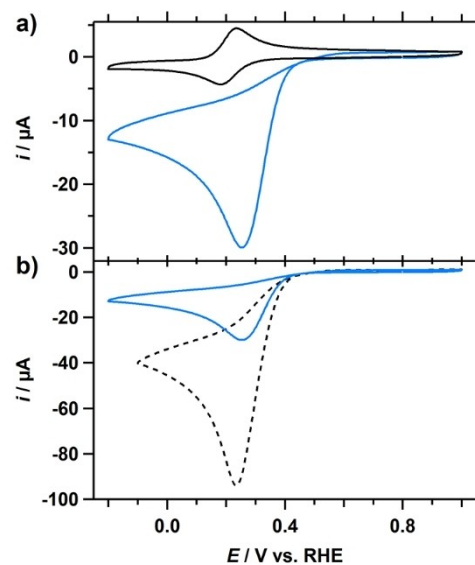


Figure 1. a) CVs of Cu-tmpa (0.30 mM) in the presence of 1 atm Ar (black) or 1.1 mM H₂O₂ (blue). $E_{\text{cat}/2} = 0.34$ V vs. RHE. b) Comparison of CVs of 1.1 mM H₂O₂ (blue) and 1 atm O₂ (dashed) reduction by Cu-tmpa (0.30 mM). Conditions: pH 7 PB ([PO₄]³⁻ = 100 mM), 293 K, 100 mV s⁻¹ scan rate, 0.0707 cm² electrode surface area.

explained by the difference in catalytic electron transfer number n of the reaction and the diffusion coefficient D of the substrate. Thus, considering the different electron transfer number for the ORR ($n = 4$) and the HPRR ($n = 2$), a D_{O_2} of 2×10^{-5} cm² s⁻¹, and a $D_{\text{H}_2\text{O}_2}$ of $0.6\text{--}1.4 \times 10^{-5}$ cm² s⁻¹,^[16] an expected ratio between the respective peak catalytic currents ($i_{\text{cat,H}_2\text{O}_2}/i_{\text{cat,O}_2}$) can be determined. If the HPRR is limited in H₂O₂ concentration, as was the case for O₂ during the ORR for this catalyst,^[7a] and i_{cat} is therefore not only determined by the catalytic rate constant or catalyst concentration, a $i_{\text{cat,H}_2\text{O}_2}/i_{\text{cat,O}_2}$ ratio in the range of 0.27 to 0.42 is expected. The $i_{\text{cat,H}_2\text{O}_2}/i_{\text{cat,O}_2}$ derived from the CVs in Figure 1b falls within the calculated ratio, indicating that the HPRR is also limited in substrate concentration at 1.1 mM H₂O₂ and a Cu-tmpa concentration of 0.3 mM.

2.2. Catalyst Concentration HPRR Dependence

The relationship between the catalytic current and the catalyst concentration was investigated by determining the peak catalytic current at a low catalyst concentration range (1.0–2.5 μM), in the presence of 1.1 mM H₂O₂. While the GC electrode showed no activity towards the reduction of H₂O₂, background correction was applied to the CV to remove contributions from the GC double layer with a magnitude of 0.5 to 1 μA . The resulting linear sweep voltammograms (LSV) are shown in Figure 2a. For each Cu-tmpa concentration, the peak current is visible around 0.23 V vs. RHE, with an $E_{\text{cat}/2}$ at 0.31 V. Both potentials have shifted closer to the redox potential of the catalyst compared to the E_{cat} and $E_{\text{cat}/2}$ observed at high catalyst concentration, which is expected when substrate diffusion limitations play a reduced role during catalysis. For the HPRR, a

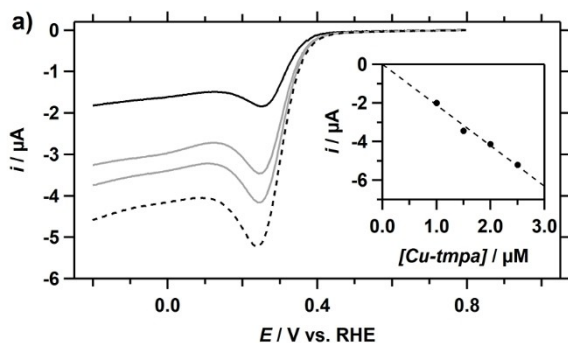


Figure 2. a) Background corrected linear sweep voltammograms (LSV) of the reduction of H_2O_2 (1.1 mM) for different concentrations of Cu-tmpa; 1.0 (solid black)/1.5/2.0/2.5 (dashed) μM . Inset: the peak catalytic current i_{cat} measured at 0.23 V vs. RHE plotted against the catalyst concentration. Conditions: pH 7 PB ($[\text{PO}_4] = 100 \text{ mM}$), 293 K, 100 mV s^{-1} scan rate.

linear relationship is observed between the i_{cat} and the Cu-tmpa concentration (Figure 2b), as was also shown for the Cu-tmpa catalysed ORR.^[7a] A plot of $\log(i_{\text{cat}})$ as a function of the logarithm of the catalyst concentration has a slope of 1.05 ($R^2 = 0.96$), confirming the first-order nature of the catalytic reaction (see Figure S1 in the Supporting Information). Additionally, the same experiment performed at a higher H_2O_2 concentration of 10 mM over a Cu-tmpa concentration range from 1 to 10 μM showed the same first-order dependence in catalyst concentration (see Figure S2).

2.3. Relationship between Hydrogen Peroxide Concentration and Catalytic Activity

As opposed to O_2 , it is far more straightforward to increase the concentration of H_2O_2 in the solution to study the relationship between the substrate concentration and the catalytic reaction. CVs were measured in a PB pH 7 electrolyte solution containing Cu-tmpa and different H_2O_2 concentrations ranging from 1.1 to 30 mM. These CVs show the familiar peak shaped catalytic wave around 0.25 V vs. RHE (Figure 3a), but from a H_2O_2 concentration of 20 mM and upwards a shoulder or second reduction event appears below 0.1 V in the CV, and becomes clearly visible at 30 mM. Expanding the concentration range to 100 mM shows that the peak current of this second catalytic wave steadily increases with the increasing H_2O_2 concentration, while the peak current of the first catalytic remains the same. Moreover, the potential at which the peak catalytic current of this reduction is reached also shifts more negatively with increasing concentration. Another observation is that an oxidation event appears in the positive potential window above 0.6 V vs. RHE at H_2O_2 concentrations of 40 mM and higher (Figure S3a). Although this oxidation could be the result of scanning to a lower potential, both the 30 and 40 mM H_2O_2 measurements have the same potential window, yet this oxidation is only present in the CVs corresponding to the solution containing 40 mM H_2O_2 and higher. Therefore, it is more likely that the observed oxidation is related to the

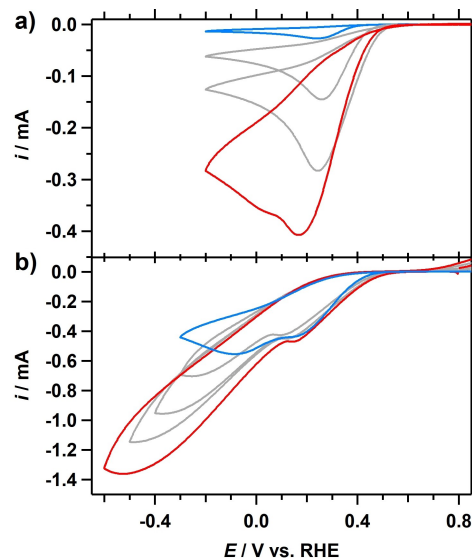


Figure 3. CVs of the reduction of H_2O_2 in the presence of 0.3 mM Cu-tmpa for a range of H_2O_2 concentrations under 1 atm Ar; a) 1.1 (blue)/5.0/10/20 (red) mM, b) 30 (blue)/40/60/80/100 (red) mM. Conditions: pH 7 PB ($[\text{PO}_4] = 100 \text{ mM}$), 293 K, 100 mV s^{-1} scan rate.

increased peroxide concentration. The onset of this catalytic oxidation is close to the standard reduction potential for the oxidation of H_2O_2 to O_2 ($E^0 = 0.695 \text{ V vs. RHE}$), making the 2-electron oxidation of H_2O_2 the most likely candidate for the observed H_2O_2 -concentration dependent oxidation. The GC electrode is not able to activate H_2O_2 in neutral solution at these low potentials, as it was only shown to catalyse the oxidation above 1.4 V vs. RHE in a PB pH 7.4 buffer (though at 1.0 mM H_2O_2),^[17] while under basic conditions ($> \text{pH } 10$) oxidation was observed above 0.9 V vs. RHE while rotating (250 mM H_2O_2).^[18] To confirm this, CVs were measured with a GC electrode in a PB pH 7 electrolyte solutions containing H_2O_2 concentrations ranging from 1.5 to 500 mM (Figure S3b). No anodic currents were observed in the absence of Cu-tmpa, showing the involvement of the copper complex in apparent oxidation of H_2O_2 .

A plot of the peak catalytic current i_{cat} derived from the obtained CVs versus the H_2O_2 concentration, reveals two different regimes where reduction of dioxygen takes place (Figure 4a). A linear relationship between i_{cat} and the concentration is apparent at low concentrations of H_2O_2 , but above 30 mM the catalytic current of the first reductive wave is no longer dependent on the substrate concentration. When the second catalytic wave at lower potential is considered, it clearly shows that the corresponding $i_{\text{cat},2}$ still has a mostly linear dependency on H_2O_2 concentration (Figure 4b), although a slight deviation from an ideal linear relationship is visible at higher concentrations. Although we cannot fully rule out that some disproportionation of peroxide may have occurred under these conditions, these results do show that the reduction reaction of H_2O_2 to water is both first-order in H_2O_2 and Cu-tmpa.

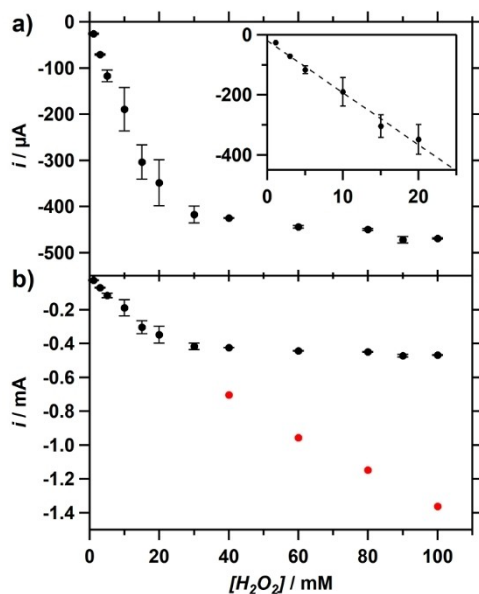


Figure 4. a) Catalytic current as a function of H_2O_2 concentration in the presence of 0.3 mM Cu-tmpa, showing a $[\text{H}_2\text{O}_2]$ dependent (zoom in inset) and independent regime. b) An expanded view including the i_{cat} values of the 2nd catalytic reduction (red circles). Conditions: pH 7 PB ($[\text{PO}_4] = 100$ mM), 293 K, 100 mV s^{-1} scan rate.

The existence of two distinct catalytic waves can be related to the buffer capacity of the electrolyte solution at pH 7. As the hydrogen peroxide concentration is approaching that of the phosphate buffer in the electrolyte solution at these higher concentrations, the buffering ability of the solution can become compromised. This would result in significantly increased pH gradient close to the electrode surface. Thus, the appearance of a second catalytic reduction at a lower potential is likely the result of a shift in proton source for the reduction of H_2O_2 to H_2O , possibly from H_2O or even H_2O_2 itself, as the pK_a of hydrogen peroxide is 11.75 in water.^[19]

2.4. Kinetic Isotope Effect Studies of the Peroxide Reduction Reaction

To get more insight into the rate-determining step in the mechanism of the electrocatalytic reduction of H_2O_2 , solvent kinetic isotope effects (KIE) were determined. Cyclic voltammograms were measured in a 0.1 M phosphate buffer (pH 7) solution containing 0.3 mM Cu-tmpa. Both deuterated and non-deuterated phosphate buffers contained the same concentration and ratio of phosphate salts (0.1 M). The pH^* , defined as the apparent pH directly determined from a H_2O calibrated pH meter in a D_2O solution, of the deuterated solution was determined to be 7.13. Using Eq. (1) to convert the pH^* to the pH ,^[20] this pH^* value corresponds to a pH of 7.03. This agrees well with the pH of 7.01 that was measured for the non-deuterated electrolyte solution. The pD can in turn be calculated using Eq. (2), resulting in a pD of 7.58.

$$\text{pH} = 0.929 \times \text{pH}^* + 0.41 \quad (1)$$

$$\text{pD} = \text{pH}^* + 0.45 \quad (2)$$

In the presence of 1 atm argon, and in the absence of hydrogen peroxide, the $E_{1/2}$ of the Cu-tmpa redox couple is positively shifted by 37 mV in the deuterated phosphate buffer compared to the non-deuterated phosphate buffer (Figure 5a). Saturating the deuterated electrolyte solution in the RHE compartment with H_2 instead of D_2 is the likely cause of this, the observed potential shift being similar to the difference in equilibrium potential E^0 for the H^+/H_2 and D^+/D_2 couples.^[21] Upon the addition of 1.1 mM H_2O_2 to the electrolyte solutions, a clear difference in catalytic rates can be observed between the deuterated and non-deuterated electrolyte solutions (Figure 5b). As with the redox couple in the absence of substrate, the $E_{\text{cat}/2}$ of the catalytic wave is positively shifted by 37 mV in the deuterated solution. More striking is the decrease of the peak catalytic current i_{cat} in the deuterated solution, from 30 to $20 \mu\text{A}$.

Conversely, when the catalytic activity of Cu-tmpa towards the ORR in deuterated PB (pH 7) electrolyte solution in the presence of 1 atm O_2 is investigated by cyclic voltammetry

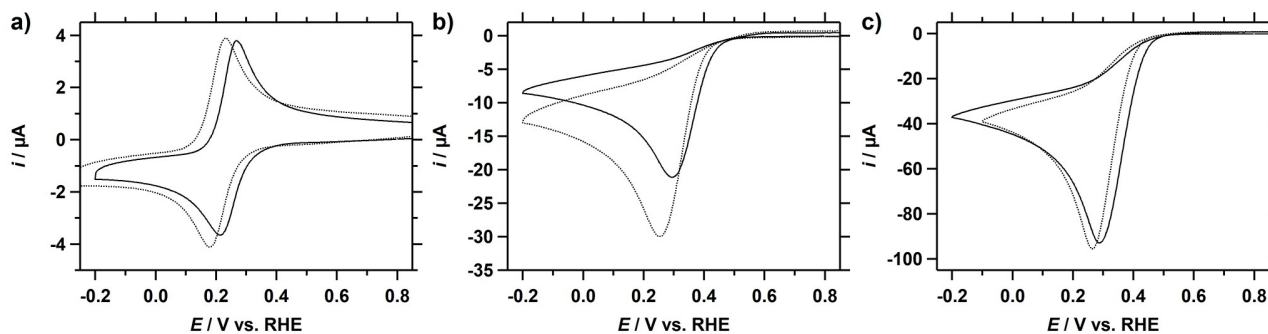


Figure 5. a) CVs of 0.3 mM Cu-tmpa under 1 atm Ar in a deuterated (solid) and non-deuterated (dotted) PB electrolyte solution. b) CVs of the catalytic reduction of H_2O_2 (1.1 mM under 1 atm Ar) by Cu-tmpa in a deuterated (solid) and non-deuterated (dotted) PB solution. c) CVs of the catalytic reduction of O_2 (1 atm) by Cu-tmpa (0.3 mM) in a deuterated (solid) and non-deuterated (dotted) PB solution. Conditions: pH 7 PB ($[\text{PO}_4] = 100$ mM), 293 K, 100 mV s^{-1} scan rate.

(Figure 5c), the catalytic half-wave potential $E_{\text{cat}/2}$ is again shifted positively by 37 mV. The difference of the i_{cat} between the deuterated solution and the non-deuterated solution is only 5 μA , which is insignificant compared to the difference observed for the H_2O_2 reduction. This is in line with the observations that the electrocatalytic ORR by Cu-tmpa is severely rate-limited in the mass-transport of O_2 at a Cu-tmpa concentration of 0.3 mM,^[7a] and suggests that this is the case in both non-deuterated and deuterated electrolyte solutions.

The KIE is defined as the ratio between the catalytic rate constants in aqueous and deuterated solutions. The electrocatalytic rate constant is directly proportional to the catalytic current enhancement, e.g. the squared ratio of i_{cat} over i_p , where the i_p is the peak reductive current of the Cu^{II} redox couple. Thus, the KIE can be determined by applying Eq. (3) to the values obtained from the CVs under both conditions.

$$\text{KIE} = \frac{k_{\text{obs,H}}}{k_{\text{obs,D}}} \propto \frac{(i_{\text{cat}}/i_p)_{\text{H}}^2}{(i_{\text{cat}}/i_p)_{\text{D}}^2} \quad (3)$$

This resulted in a solvent KIE value of 1.65 for the reduction of hydrogen peroxide, which indicates that proton transfer is involved in the rate-determining step of the catalytic reaction. While the determined KIE value is not particularly large, it is in the range of KIEs that are associated with homolytic cleavage of the O–O bond of the $\text{Cu}^{\text{II}}\text{--OOH}$, in conjunction with a proton transfer.^[22] However, it was shown that the HPRR by Cu-tmpa is mass-transport limited in H_2O_2 under the experimental conditions used here, which may result in an underestimation of the KIE that was obtained from i_{cat} derived directly from the CVs in Figure 5b. Directly deriving the rate constants under non mass-transport limiting conditions, will result in a more accurate determination of the KIE.

2.5. Reaction Kinetics and FOWA of the HPRR

While a quick analysis of cyclic voltammograms of the ORR and HPRR by Cu-tmpa (Figure 1b) already reveals that HPRR by Cu-tmpa is significantly slower than ORR under the same catalytic conditions and substrate concentrations, the rate constants of the reaction can be determined via foot-of-the-wave analysis (FOWA) or by direct determination using the catalytic current enhancement. Using the FOWA method to determine rate constants, only the beginning of the catalytic wave is used, a region which is not affected by substrate consumption, catalyst deactivation, product inhibition or other side phenomena. In this way the ideal or maximum turnover frequency (TOF_{max}) associated with the catalytic reaction can be determined. The FOWA has been described in detail previously by Savéant, Costentin and others.^[23]

For the FOWA (see Supporting Information, section 1.3), a CV was measured in triplicate in a PB (pH 7) electrolyte solution containing 0.3 mM Cu-tmpa and 1.1 mM H_2O_2 , using a freshly polished GC electrode. The resulting CVs are shown in Figure S4a. From these CVs, plots of the current enhancement i_c/i_p vs. $\exp[-F/RT(E - E_{1/2})]$ were constructed (Figure S4c). Here, i_c

is the current associated with the catalytic HPRR reaction at the applied potential E and i_p is the peak cathodic current associated with the Cu^{II} redox couple of Cu-tmpa. In the foot-of-the-wave region, a linear fit (Figure S4e; $R^2 > 0.98$) was applied between the onset of the HPRR and the potential at which i_c/i_p is at least larger than 1.6, i.e. the potential where the catalytic current is 60% larger than the peak cathodic current of the Cu^{II} redox couple. The catalytic onset is defined as $i_c/i_{\text{redox}} \geq 2$, where i_{redox} is the current associated with the reduction of the catalyst measured at the applied potential E , in the absence of H_2O_2 . From the slope of the linear fit, the TOF_{max} for the HPRR by Cu-tmpa in pH 7 phosphate buffer solution containing 1.1 mM H_2O_2 was determined to be $2.1 \times 10^5 \pm 0.1 \times 10^5 \text{ s}^{-1}$. This is one order of magnitude (9 times) less than was previously reported for the ORR (Figure 6a).^[7a] Using the same approach, the TOF_{max} for the HPRR in the deuterated pH 7 phosphate buffer solution was determined to be $1.5 \times 10^5 \pm 0.1 \times 10^5 \text{ s}^{-1}$. A comparison of the TOF_{max} of the HPRR in H_2O and D_2O is shown in Figure 6b and confirms that the Cu-tmpa catalysed HPRR is indeed slower in D_2O . By applying Eq. (3), where TOF_{max} was used as the k_{obs} , a KIE of 1.37 ± 0.14 was calculated.

$$\frac{i_{\text{cat}}}{i_p} = 2.24n_{\text{cat}} \sqrt{\frac{RT}{Fv}} k_{\text{obs}} \quad (4)$$

$$i_p = 0.446n_{\text{cat}} F C_{\text{cat}}^0 \sqrt{\frac{Fv}{RT}} D_{\text{cat}} \quad (5)$$

A more direct approach to obtain a rate constant can be achieved by using the catalytic current enhancement i_{cat}/i_p and applying Eq. (4), where R , T and F are known constants, v is the scan rate (V/s), and n_{cat} is the number of electrons transferred during the catalytic reaction.^[24] The current enhancement was determined from the background-corrected peak catalytic current i_{cat} at low catalyst concentration (1.0–2.5 μM) in the presence of 1.1 mM H_2O_2 , as discussed in a previous section. No redox current is visible above the double layer current at these low catalyst concentrations. Therefore, for each catalyst concentration the i_p was calculated using the diffusion coefficient of Cu-tmpa ($D = 4.9 \times 10^{-6} \text{ cm}^2 \text{ s}^{-1}$) by applying the Randles-Sevcik

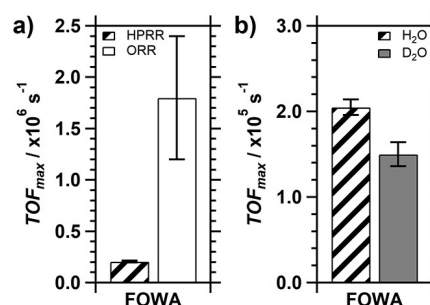


Figure 6. a) Comparison between the TOF_{max} of Cu-tmpa for the HPRR (1.1 mM H_2O_2 under 1 atm Ar) and the ORR (1 atm O_2) as determined by FOWA. b) Comparison between the TOF_{max} of the HPRR in H_2O and D_2O . Conditions: [Cu-tmpa] = 0.3 mM, pH 7 PB ($[\text{PO}_4] = 100 \text{ mM}$), 293 K, 100 mV s^{-1} scan rate.

equation [Eq. (5)]. This resulted in a k_{obs} of $4.8 \times 10^3 \pm 0.4 \times 10^3 \text{ s}^{-1}$ (Figure 7). Repeating the same experiments in deuterated electrolyte solutions resulted in a k_{obs} of $3.2 \times 10^3 \pm 0.4 \times 10^3 \text{ s}^{-1}$. Equation 3 was applied to these catalytic rate constants giving a KIE of 1.48 ± 0.17 , showing that at both low and high catalyst concentration, and under both substrate limited and non-limiting conditions, a significant kinetic isotope effect is observed.

3. Discussion

As demonstrated, the electrocatalytic HPRR by Cu-tmpa is a first-order reaction in both the catalyst and the hydrogen peroxide substrate. Using FOWA, the TOF_{max} for the reduction of H_2O_2 was shown to be one order of magnitude lower than that of the 2-electron reduction of O_2 to H_2O_2 , consistent with the analysis of the Tafel slopes for ORR and HPRR previously reported by us.^[7a] The HPRR k_{obs} ($4.8 \times 10^3 \text{ s}^{-1} \pm 0.4 \times 10^3 \text{ s}^{-1}$) that was obtained at low catalyst concentration was significantly lower than the FOWA-derived TOF_{max} ($2.1 \times 10^5 \text{ s}^{-1} \pm 0.1 \times 10^5 \text{ s}^{-1}$) at higher catalyst concentration. Such a $k_{\text{obs}} < \text{TOF}_{\text{max}}$ is expected due to previously mentioned deviations from an ideal catalytic system.

However, the difference between the k_{obs} and the TOF_{max} of the HPRR is significantly larger (2.5 times) than the difference between the k_{obs} ($1.5 \times 10^5 \text{ s}^{-1}$) and TOF_{max} ($1.8 \times 10^6 \text{ s}^{-1}$) of the ORR that we have previously reported.^[7a] A few factors can explain this difference. Firstly, during the ORR the partial 2-electron reduction of O_2 to H_2O_2 and the 2-electron reduction of H_2O_2 both contribute to the peak catalytic current, each with a different catalytic rate. Thus, the intermediate H_2O_2 is generated in situ near the electrode surface, thereby minimizing the effect of mass-transport of H_2O_2 to the electrode on the subsequent 2-electron reduction to H_2O . Given that the diffusion constant of H_2O_2 ($0.6\text{--}1.4 \times 10^{-5} \text{ cm}^2 \text{ s}^{-1}$) is significantly lower than that of O_2 ($2.0 \times 10^{-5} \text{ cm}^2 \text{ s}^{-1}$), this would enhance the catalytic current associated with the reduction of H_2O_2 , contributing to a higher overall k_{obs} for the 4-electron ORR as determined via the current

enhancement (CE) $i_{\text{cat}}/i_{\text{p}}$. This would result in a smaller difference between the k_{obs} and TOF_{max} for the ORR, where the latter is derived from the partial 2-electron reduction of O_2 . Conversely, for the HPRR both the FOWA and CE rate constants are associated with the same 2-electron reduction of H_2O_2 . During the HPRR diffusion of H_2O_2 to the electrode does play a role and does not benefit of an increased catalytic rate due to in situ generation of the substrate that resulted in a smaller difference between the k_{obs} and TOF_{max} for the ORR.

Furthermore, in the case of the HPRR, one of the contributing factors to the observed deviation from the ideal behaviour can be related to catalysts decomposition or deposition. Indeed, prolonged cycling during CV measurements shows a significant change in shape of the catalytic events (see Figure S5 in the Supporting Information), followed by increased activity after mixing and saturating the solution with argon, something that was not observed for the ORR. During ORR, the reduction of H_2O_2 is only expected under conditions wherein the overall reduction reaction is nearly mass transport limited in O_2 . Under such conditions one would not expect to find a large deviation from the ideal catalytic activity due to catalyst degradation, if one considers that catalyst deactivation is linked to the reduction of H_2O_2 and not to the 2-electron reduction of O_2 .

The mechanism for H_2O_2 reduction on copper has been proposed to go through a Fenton-type mechanism, based on research on copper monooxygenases or on bio-inspired copper complexes as monooxygenase mimics.^[9] In this mechanism, it is proposed that the O–O bond of hydrogen peroxide is split homolytically. This can either result in a copper oxyl radical (Cu-O^{\bullet}) and a free hydroxyl anion (HO^-), or a copper hydroxyl species (Cu-OH) and a free hydroxyl radical anion (HO^{\bullet}) as intermediates. For LPMO, it has been found by computational methods that the latter route is more favourable.^[25] Additionally, it was shown that the hydroxyl radical was stabilized in the enzyme binding pocket of the active site, preventing damage caused by free radical species. This allows for a hydrogen atom abstraction (HAA) by the hydroxyl radical from the copper bound hydroxyl group, resulting in Cu-O^{\bullet} and a water molecule.^[9b] These possible catalytic pathways are schematically shown in Scheme 1, which also includes an outer sphere electron-transfer PCET step as an alternative for the HAA.^[26] In an electrochemical system, where electron transfer is very fast, and no free radical-stabilizing binding pocket is available, outer sphere electron transfer mediated by the solvent and/or phosphate ions should be considered.

The solvent kinetic isotope effect of 1.4–1.7 for the HPRR catalysed by Cu-tmpa indicates that bond breaking of an O–H bond is involved in the rate-determining step of the catalytic reaction. The relatively low KIE would suggest a weak O–H bond with little covalent character is involved. Solvent KIEs in the same range were observed for an Fe(III)-hydroperoxide porphyrin model for the active site of heme oxygenase.^[22b,c,27] Based on computational methods, the solvent KIE was proposed to be associated with a concerted, stepwise mechanism of proton transfer from the $\text{H}_2\text{O}/\text{H}_3\text{O}^+$ and solvent O–O bond breaking, while involving a rearrangement of the formed

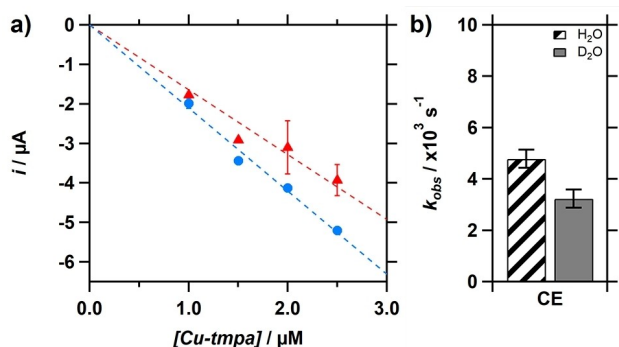
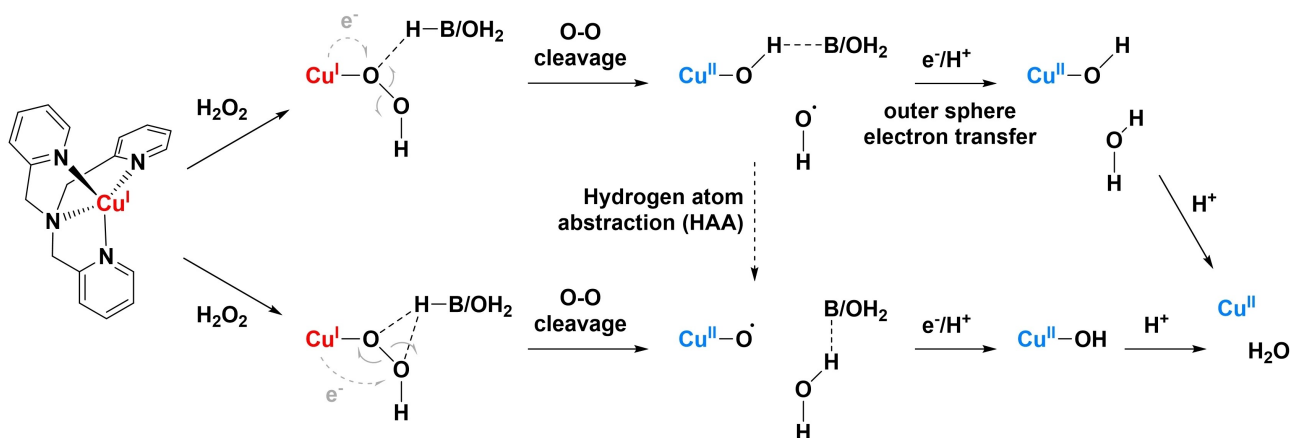


Figure 7. a) The peak catalytic current i_{cat} plotted against the Cu-tmpa concentration in a deuterated (red triangles) and non-deuterated (blue circles) PB electrolyte solution containing 1.1 mM H_2O_2 under 1 atm Ar. b) Comparison for the k_{obs} derived from the current enhancement (CE) between the hydrogen peroxide reduction in H_2O and D_2O . Conditions: pH 7 PB ($[\text{PO}_4] = 100 \text{ mM}$), 293 K, 100 mV s^{-1} scan rate.



Scheme 1. Possible electrocatalytic HPRR pathways in the presence of Cu-tmpa, showing a pathway that proceeds via a Cu hydroxyl and free hydroxyl radical (top), or via copper oxyl radical (bottom). In copper monooxygenases, the possibility of an HAA step has been proposed, enabled by the stabilizing effect of the binding pocket on the hydroxyl radical (see text).

hydroxyl radical anion. Such a mechanism would align closer with the top route shown in Scheme 1. The resulting free hydroxyl radical anion would also explain the observed instability of the complex under catalytic conditions, as it could react with the tmpa ligand.

4. Conclusions

The catalytic performance was investigated of Cu-tmpa for the electrocatalytic reduction of H_2O_2 in pH 7 phosphate buffered neutral aqueous solution. It was confirmed that the reduction of H_2O_2 is significantly slower than O_2 reduction, with rate constants being 10 (TOF_{max}) to 30 (k_{obs}) times lower. As is the case for the ORR, the HPRR displayed a first-order dependence on the catalyst concentration, showing that only a single copper site is involved in the catalytic reaction, which fits well with the reported literature on iron- and copper-catalysed H_2O_2 reduction in enzymes. Additionally, the reaction shows a first-order dependence on the H_2O_2 concentration as well, up until the buffering capacity of the 0.1 M PB buffer is compromised. The effect on the catalytic performance by using D_2O as the solvent was studied, and resulted in a solvent KIE between 1.4–1.7 for the HPRR. However, while this does confirm that a hydrogen or proton transfer is involved in the rate-determining step of the catalytic reaction, the magnitude of the KIE alone does not allow us to pinpoint the exact mechanistic route for the HPRR. Yet, when combining what is known about copper monooxygenases with the obtained solvent KIE and the apparent instability of the Cu-tmpa under catalytic HPRR conditions, the pathway in which free hydroxyl radical anions are formed seems the most likely candidate at this point.

Experimental Section

General

Aqueous electrolyte solutions were prepared using NaH_2PO_4 (Suprapur[®], Merck) and Na_2HPO_4 (Suprapur[®], Merck). $[\text{Cu}(\text{tmpa})(\text{CH}_3\text{CN})](\text{OTf})_2$ was synthesized as previously reported.^[7a] Milli-Q Ultrapure grade water was used for all electrochemical experiments and for the preparation of all aqueous electrolyte solutions. D_2O for the kinetic isotope experiments was obtained from Sigma-Aldrich (99.9 atom% D). H_2O_2 was obtained from Sigma-Aldrich ($\geq 30\%$, for ultratrace analysis), and the exact concentration was determined via permanganate titration. Alumina suspensions (1.0, 0.3, and 0.05 μm) were obtained from Buehler. pH measurements were done using a Hanna Instruments HI 4222 pH meter which was calibrated by five-point calibration using IUPAC standard buffers. All gasses used during electrochemical measurements, H_2 , O_2 , and argon (each 5.0 grade), were supplied by Linde.

Electrochemical measurements

All electrochemical experiments were performed in a custom-built 10 mL single-compartment glass cell with a three-electrode setup. The measurements were performed using Autolab PGSTAT 12, 204, and 128N potentiostats, operated by the Autolab NOVA 2 software. The working electrodes were glassy carbon (GC) disks, either a GC rod ($A=0.071\text{ cm}^2$, type 1, Alfa Aesar) in hanging meniscus configuration, or a PEEK encapsulated GC disk ($A=0.071\text{ cm}^2$, Metrohm) submerged in the solution. Unless otherwise stated, the GC electrodes were manually polished before each catalytic measurement for 5 mins with 1.0, 0.3, and 0.05 μm alumina suspensions on Buehler cloth polishing pads, or with a Struers LaboPol-30 polishing machine using 1.0 μm diamond and 0.04 μm silica suspension on polishing cloths (Dur-type) for 1 min each. This was followed by sonication of the electrode in Milli-Q purified water for 10–15 minutes. A gold wire was used as a counter electrode and was flame annealed and rinsed with Milli-Q purified water. The reference electrode was a reversible hydrogen electrode (RHE) made from a Pt mesh submerged in same electrolyte solution as the main cell compartment, connected via a Luggin capillary, and continuously sparged with H_2 gas. Oxygen-free electrolyte solutions were prepared by saturating the cell for 20 to 30 minutes with Ar, after which an atmosphere of 1 atm Ar was maintained. Oxygen-saturated electrolyte solutions were obtained by saturating the cell

for 20 minutes with O₂, after which a 1 atm O₂ atmosphere was maintained. All glassware was regularly cleaned by submersion in an aqueous oxidizing solution containing 0.5 M H₂SO₄ and 1 mg/mL (6.3 mM) KMnO₄ overnight. This is followed by removal of excess KMnO₄ and MnO₂ from the glassware with diluted H₂SO₄ and H₂O₂, followed by rinsing the glassware three times with water and boiling twice submerged in Milli-Q purified water.

Electrochemical measurements in D₂O

In preparation of the measurements in D₂O, all glassware was cleaned following the procedure described previously. Additionally, the glassware was dried in an oven at 140 °C for 2 days. The GC working electrode was polished as previously described, followed by sonication in D₂O instead of H₂O. After each polishing cycle and before every measurement, the GC electrode was submerged in the deuterated electrolyte solution for at least 2 minutes. Both the counter and reference electrode were flame annealed and rinsed with D₂O before the experiment. The electrolyte solutions were prepared by weighing the required phosphate salts (NaH₂PO₄ and Na₂HPO₄), which were stored under vacuum in a desiccator containing aluminosilicate drying pearls, in a 100 mL volumetric flask. The volumetric flask was filled to 100 mL with D₂O. The apparent pH* was measured using a calibrated pH meter filled with non-deuterated electrolyte solution. Both the main cell compartment and the Luggin compartment containing the RHE electrode were filled with the same deuterated PB solution. Catalyst solutions were obtained by first drying Cu-tmpa on a Schlenk-line overnight, before weighing the required amount. This was followed by preparation of concentrated stock solutions of Cu-tmpa (30.0 mM) in D₂O for use in the electrochemical experiments. H₂O₂ (10.0 M in H₂O) was used as is, as the maximum proton content during the electrochemical measurements would not exceed 0.01 %.

Acknowledgements

Financial support was provided by the European Research Council (ERC starting grant 637556 Cu4Energy to D.G.H.H.).

Conflict of Interest

The authors declare no conflict of interest.

Keywords: copper · electrocatalysis · hydrogen peroxide · hydroxyl radicals · mechanistic studies

- [1] a) G. Grigoropoulou, J. H. Clark, J. A. Elings, *Green Chem.* **2003**, *5*, 1–7; b) R. Noyori, M. Aoki, K. Sato, *Chem. Commun.* **2003**, 1977–1986; c) A. Goti, F. Cardona, P. Tundo, V. Esposito, *Green Chemical Reactions*, Springer Netherlands, Dordrecht, **2008**, pp. 191–212; d) A. Podgoršek, M. Zupan, J. Iskra, *Angew. Chem. Int. Ed.* **2009**, *48*, 8424–8450; *Angew. Chem.* **2009**, *121*, 8576–8603.
- [2] a) V. Prabhakaran, C. G. Arges, V. Ramani, *Proc. Nat. Acad. Sci.* **2012**, *109*, 1029–1034; b) D. E. Curtin, R. D. Lousenberg, T. J. Henry, P. C. Tangeman, M. E. Tisack, *J. Power Sources* **2004**, *131*, 41–48; c) Y. Wang, K. S. Chen, J. Mishler, S. C. Cho, X. C. Adroher, *Appl. Energy* **2011**, *88*, 981–1007; d) L. An, T. Zhao, X. Yan, X. Zhou, P. Tan, *Sci. Bull.* **2015**, *60*, 55–64.
- [3] a) K. Asada, *Physiol. Plant.* **1992**, *85*, 235–241; b) E. Nagababu, F. J. Chrest, J. M. Rifkind, *Biochim. Biophys. Acta Gen. Subj.* **2003**, *1620*, 211–217.
- [4] a) D. Maiti, A. A. Narducci Sarjeant, K. D. Karlin, *Inorg. Chem.* **2008**, *47*, 8736–8747; b) A. Ghosh, D. A. Mitchell, A. Chanda, A. D. Ryabov, D. L. Popescu, E. C. Upham, G. J. Collins, T. J. Collins, *J. Am. Chem. Soc.* **2008**, *130*, 15116–15126; c) B. J. Day, *Biochem. Pharmacol.* **2009**, *77*, 285–296; d) A. Tovmasyan, C. G. C. Maia, T. Weitner, S. Carballal, R. S. Sampaio, D. Lieb, R. Ghazaryan, I. Ivanovic-Burmazovic, G. Ferrer-Sueta, R. Radi, J. S. Reboucas, I. Spasojevic, L. Benov, I. Batinic-Haberle, *Free Radical Biol. Med.* **2015**, *86*, 308–321; e) S. Signorella, C. Palopoli, G. Ledesma, *Coord. Chem. Rev.* **2018**, *365*, 75–102.
- [5] a) G. Vaaje-Kolstad, B. Westereng, S. J. Horn, Z. Liu, H. Zhai, M. Sørli, V. G. H. Eijsink, *Science* **2010**, *330*, 219–222; b) S. J. Horn, G. Vaaje-Kolstad, B. Westereng, V. G. Eijsink, *Biotechnol. Biofuels* **2012**, *5*, 45–45; c) G. Vaaje-Kolstad, Z. Forsberg, J. S. M. Loose, B. Bissaro, V. G. H. Eijsink, *Curr. Opin. Struct. Biol.* **2017**, *44*, 67–76; d) G. R. Hemsworth, E. M. Johnston, G. J. Davies, P. H. Walton, *Trends Biotechnol.* **2015**, *33*, 747–761; e) F. Calderaro, M. Keser, M. Akeroyd, L. E. Bevers, V. G. H. Eijsink, A. Várnai, M. A. van den Berg, *Biotechnol. Biofuels* **2020**, *13*, 195.
- [6] L. Ciano, G. J. Davies, W. B. Tolman, P. H. Walton, *Nat. Catal.* **2018**, *1*, 571–577.
- [7] a) M. Langerman, D. G. H. Hetterscheid, *Angew. Chem. Int. Ed.* **2019**, *58*, 12974–12978; *Angew. Chem.* **2019**, *131*, 13108–13112; b) N. W. G. Smits, B. van Dijk, I. De Bruin, S. L. T. Groeneveld, M. A. Siegler, D. G. H. Hetterscheid, *Inorg. Chem.* **2020**, *59*, 16398–16409; c) M. A. Thorseth, C. S. Letko, T. B. Rauchfuss, A. A. Gewirth, *Inorg. Chem.* **2011**, *50*, 6158–6162; d) S. Kakuda, R. L. Peterson, K. Ohkubo, K. D. Karlin, S. Fukuzumi, *J. Am. Chem. Soc.* **2013**, *135*, 6513–6522; e) R. Venegas, K. Muñoz-Becerra, L. Lemus, A. Toro-Labbé, J. H. Zagal, F. J. Recio, *J. Phys. Chem. C* **2019**, *123*, 19468–19478; f) K. Muñoz-Becerra, D. F. Báez, J. H. Zagal, S. Bollo, A. Toro-Labbé, R. Venegas, F. J. Recio, *Electrochim. Acta* **2020**, *357*, 136881.
- [8] J. A. Hangasky, M. A. Marletta, *Biochemistry* **2018**, *57*, 3191–3199.
- [9] a) S. Kim, J. W. Ginsbach, J. Y. Lee, R. L. Peterson, J. J. Liu, M. A. Siegler, A. A. Sarjeant, E. I. Solomon, K. D. Karlin, *J. Am. Chem. Soc.* **2015**, *137*, 2867–2874; b) B. Wang, P. H. Walton, C. Rovira, *ACS Catal.* **2019**, *9*, 4958–4969.
- [10] a) R. L. Lieberman, A. C. Rosenzweig, *Nature* **2005**, *434*, 177–182; b) R. A. Himes, K. D. Karlin, *Curr. Opin. Chem. Biol.* **2009**, *13*, 119–131; c) S. M. Smith, S. Rawat, J. Telsner, B. M. Hoffman, T. L. Stemmler, A. C. Rosenzweig, *Biochemistry* **2011**, *50*, 10231–10240; d) L. Cao, O. Calderaru, A. C. Rosenzweig, U. Ryde, *Angew. Chem. Int. Ed.* **2018**, *57*, 162–166; *Angew. Chem.* **2018**, *130*, 168–172; e) M. Miyanishi, T. Abe, Y. Hori, Y. Shiota, K. Yoshizawa, *Inorg. Chem.* **2019**, *58*, 12280–12288.
- [11] M. O. Ross, F. MacMillan, J. Wang, A. Nisthal, T. J. Lawton, B. D. Olafson, S. L. Mayo, A. C. Rosenzweig, B. M. Hoffman, *Science* **2019**, *364*, 566–570.
- [12] a) W. Liu, D. Zuckerbrod, *J. Electrochem. Soc.* **2005**, *152*, A1165; b) T. Kinumoto, M. Inaba, Y. Nakayama, K. Ogata, R. Umabayashi, A. Tasaka, Y. Iriyama, T. Abe, Z. Ogumi, *J. Power Sources* **2006**, *158*, 1222–1228; c) M. Inaba, T. Kinumoto, M. Kiriake, R. Umabayashi, A. Tasaka, Z. Ogumi, *Electrochim. Acta* **2006**, *51*, 5746–5753; d) K. Hongsirikarn, X. Mo, J. G. Goodwin, S. Creager, *J. Power Sources* **2011**, *196*, 3060–3072.
- [13] a) S. Fukuzumi, Y. Yamada, K. D. Karlin, *Electrochim. Acta* **2012**, *82*, 493–511; b) L. An, T. S. Zhao, X. L. Zhou, L. Wei, X. H. Yan, *RSC Adv.* **2014**, *4*, 65031–65034; c) E. Miglbauer, P. J. Wójcik, E. D. Glowacki, *Chem. Commun.* **2018**, *54*, 11873–11876; d) Y. Yang, Y. Xue, F. Huang, H. Zhang, K. Tao, R. Zhang, Q. Shen, H. Chang, *ACS Appl. Mater. Interfaces* **2018**, *1*, 5328–5335.
- [14] J. M. Campos-Martin, G. Blanco-Brieva, J. L. G. Fierro, *Angew. Chem. Int. Ed.* **2006**, *45*, 6962–6984; *Angew. Chem.* **2006**, *118*, 7116–7139.
- [15] R. Hage, A. Lienke, *Angew. Chem. Int. Ed.* **2006**, *45*, 206–222; *Angew. Chem.* **2006**, *118*, 212–229.
- [16] a) S. A. M. van Stroe-Biezen, F. M. Everaerts, L. J. J. Janssen, R. A. Tacke, *Anal. Chim. Acta* **1993**, *273*, 553–560; b) S. B. Hall, E. A. Khudaish, A. L. Hart, *Electrochim. Acta* **1999**, *44*, 2455–2462.
- [17] K. Aoki, M. Ishida, K. Tokuda, K. Hasebe, *J. Electroanal. Chem.* **1988**, *251*, 63–71.
- [18] P. Westbroek, E. Temmerman, *J. Electroanal. Chem.* **2000**, *482*, 40–47.
- [19] G. Goor, J. Glenneberg, S. Jacobi, J. Dadabhoy, E. Candido, *Ullmann's Encyclopedia of Industrial Chemistry*, pp. 1–40.
- [20] A. Krężel, W. Bal, *J. Inorg. Biochem.* **2004**, *98*, 161–166.
- [21] a) M. M. Ghoneim, S. Clouser, E. Yeager, *J. Electrochem. Soc.* **1985**, *132*, 1160–1162; b) J. Xu, W. Huang, R. L. McCreey, *J. Electroanal. Chem.* **1996**, *410*, 235–242.
- [22] a) E. Gopinath, T. C. Bruice, *J. Am. Chem. Soc.* **1991**, *113*, 4657–4665; b) R. Davydov, T. Matsui, H. Fujii, M. Ikeda-Saito, B. M. Hoffman, *J. Am. Chem. Soc.* **2003**, *125*, 16208–16209; c) D. Kumar, S. P. de Visser, S. Shaik, *J. Am. Chem. Soc.* **2005**, *127*, 8204–8213.

- [23] a) C. Costentin, S. Drouet, M. Robert, J.-M. Savéant, *J. Am. Chem. Soc.* **2012**, *134*, 11235–11242; b) C. Costentin, J.-M. Savéant, *ChemElectroChem* **2014**, *1*, 1226–1236; c) E. S. Rountree, B. D. McCarthy, T. T. Eisenhart, J. L. Dempsey, *Inorg. Chem.* **2014**, *53*, 9983–10002; d) V. Artero, J.-M. Saveant, *Energy Environ. Sci.* **2014**, *7*, 3808–3814; e) C. Costentin, J.-M. Savéant, *J. Am. Chem. Soc.* **2017**, *139*, 8245–8250.
- [24] R. M. Bullock, A. M. Appel, M. L. Helm, *Chem. Commun.* **2014**, *50*, 3125–3143.
- [25] B. Wang, E. M. Johnston, P. Li, S. Shaik, G. J. Davies, P. H. Walton, C. Rovira, *ACS Catal.* **2018**, *8*, 1346–1351.
- [26] a) N. Ramaswamy, S. Mukerjee, *J. Phys. Chem. C* **2011**, *115*, 18015–18026; b) I. Kenkel, A. Franke, M. Dürr, A. Zahl, C. Dücker-Benfer, J. Langer, M. R. Filipović, M. Yu, R. Puchta, S. R. Fiedler, M. P. Shores, C. R. Goldsmith, I. Ivanović-Burmazović, *J. Am. Chem. Soc.* **2017**, *139*, 1472–1484.
- [27] P. K. Sharma, R. Kevorkiants, S. P. de Visser, D. Kumar, S. Shaik, *Angew. Chem. Int. Ed.* **2004**, *43*, 1129–1132; *Angew. Chem.* **2004**, *116*, 1149–1152.

Manuscript received: April 1, 2021

Revised manuscript received: May 4, 2021

Accepted manuscript online: May 6, 2021